Organic Ionic Plastic Crystal/PVDF Composites Prepared by Solution Casting

Yanyu Wang, Dominic Rochefort*

Département de Chimie, Université de Montréal, 1375 Ave. Thérèse-Lavoie-Roux, Montréal, Québec, H2V 0B3, Canada

* *Corresponding author : dominic.rochefort@umontreal.ca*

Abstract

Solid-state electrolytes have been considered as a promising candidate to address the safety issues for next-generation lithium batteries. Organic ionic plastic crystals (OIPCs) are attracting increasing interest as solid electrolyte materials due to their unique advantages. In this study, an OIPC-based composite electrolyte consisting of the OIPC 1-ethyl-1-methylpyrrolidinium bis(trifluoromethylsulfonyl)imide ($Pyr_{12}TFSI$), lithium bis(trifluoromethylsulfonyl)imide (LiTFSI) and the polymer polyvinylidene fluoride (PVDF) has been developed by a facile solution casting strategy. Free-standing and flexible OIPC/polymer composite membranes were fabricated by the solution casting method, which not only provides flexibility and better electrode/electrolyte contact, but also is more compatible with current battery processing methods. The thermal behavior and ionic conductivity of the OIPC-based composites with different molar proportions (10 mol% to 67 mol%) of LiTFSI in LiTFSI/$Pyr_{12}TFSI$ as well as different weight fractions (20 wt% to 50 wt%) of PVDF were studied to understand the effect on transport properties. Among all the compositions studied, the $Li_{0.33}Pyr_{0.67}TFSI$/30wt%PVDF composite exhibited high ionic conductivity (e.g. 1.2×10^{-4} S cm^{-1} at 30 °C). The $Li_{0.33}Pyr_{0.67}TFSI$/30wt%PVDF composite membrane was evaluated in Li/Li symmetric cell and was cycled stably over 900 h at a current density of 0.1 mA cm^{-2} at 50 °C, demonstrating that this OIPC/polymer composite electrolyte enabled the reversible and stable lithium plating and stripping behaviors. Further tests of the $Li_{0.33}Pyr_{0.67}TFSI$/30wt%PVDF composite membrane as solid electrolyte in $LiFePO_4$/Li cell presented a high specific capacity of 149 mAh g^{-1} at 0.1 C and a long cycle life of over 440 cycles with capacity retention of 89% at 0.5 C at 50 °C, which showed improved rate capability and cycling stability in comparison with the composites with similar compositions but obtained by powder pressing method. This study demonstrated the potential of the OIPC/polymer

composite solid electrolyte prepared by solution casting method and will promote the development of high-performance OIPC-based composite electrolytes for solid-state batteries.

Keywords: Pyrrolidinium, OIPC, Lithium battery, Conductivity, Solid-state electrolyte, Membrane

1. Introduction

Lithium-ion batteries (LIBs) have been widely used in many applications ranging from portable electronics to electric vehicles and even large-scale electrical grids. So far traditional commercialized LIBs are heavily dependent on the utilization of volatile and flammable organic liquid solvents as electrolytes, which can trigger a series of safety issues, such as leakage, combustion, and even explosion. [1-3] To eliminate these safety concerns, replacing liquid electrolytes with solid-state electrolytes is considered as an effective solution. Meanwhile, solid-state electrolytes allow the use of lithium metal anode, which can further boost the energy density of LIBs. [1-3]

Organic ionic plastic crystals (OIPCs) are solid-state analogues of ionic liquids (ILs). As an emerging class of solid-state electrolyte materials, OIPCs have attracted growing interest in recent years due to their appealing advantages, such as plasticity, nonflammability, good thermal and electrochemical stability. [4-6] OIPCs have regular crystal structures of long-range order with short-range disorder. They generally exhibit one or more solid–solid phase transitions prior to melting with a low entropy of fusion ($\Delta S_{fusion} < 20$ J K^{-1} mol^{-1}) [7], which is associated with the orientational or rotational motions of the ions, and thereby a progressive disordered structure. The disordered feature endows OIPCs with plasticity, which facilitates ion conduction and is also desirable for solid-state electrochemical devices as it may improve the contact between electrode and electrolyte. [4-6, 8] OIPCs on their own usually have relatively low ionic conductivity (between 10^{-6} and 10^{-9} S cm^{-1}) at ambient temperature. [8-12] To be used as solid-state electrolytes in Li batteries, target Li ions must be added with the OIPCs to support charge/discharge processes, and it has been demonstrated that adding lithium salt into OIPC can significantly enhance their ionic conductivity. [8-12] Particularly, based on the fact that the

electrolytes with high Li salt concentration (> 1 M) have demonstrated the inhibition of aluminum current collector corrosion, the suppression of Li dendrite growth, higher target ion transport and better cycling performance, [13-16] OIPC-based electrolytes with high concentrations of Li salt are increasingly been studied recently. [8, 11, 17]

Unfortunately, the mixtures of OIPCs and Li salt are usually rather soft or in some cases a liquid phase is formed when Li salt is added, which makes them difficult to use alone as solid-state electrolyte. Incorporating OIPCs into a polymer matrix to form an OIPC/polymer composite electrolyte is a potential strategy that can simultaneously achieve desirable ionic conductivity, low electrode/electrolyte interfacial resistance, and sufficient mechanical strength. [18, 19] Progress has been made to develop OIPC-based composites as solid electrolytes for Li battery applications. [8, 12, 17, 20-25] For example, thin and flexible OIPC-based composites using polyvinylidene fluoride (PVDF) nanofiber matrix were prepared by electrospinning or co-electrospinning. [21-24] The Li | $LiFePO_4$ (LFP) cell using such OIPC-based composites delivered a capacity of 140 mA h g^{-1} at C/15 and 80 °C. [21-24] It was also evidenced that the interfacial reaction between PVDF and OIPC promoted a more disordered interphase, which facilitated ion mobility and contributed to the ionic conductivity enhancement. [21-24] However, the random distribution of the electrospun nanofiber results in an inhomogeneous interfacial area between the polymer and OIPCs, which plays an important role in ion transport in the composite. To better control the interfacial area, Howlett's group proposed to use PVDF nanoparticles to prepare the OIPC-based composites by an easier powder pressing method. The OIPC/polymer composite electrolyte prepared using this approach with N-ethyl-N-methylpyrrolidinium bis(fluorosulfonyl)imide ($Pyr_{12}FSI$), lithium bis(fluorosulfonyl)imide (LiFSI), and PVDF nanoparticles exhibited relatively high ionic conductivity (10^{-4} S cm^{-1} at 30 °C) and high Li^+ transference number (0.44 ± 0.02 at 50 °C). The applicability of these

composites was demonstrated in the Li/$LiNi_{1/3}Mn_{1/3}Co_{1/3}O_2$ (NMC) cells which showed a better capacity retention of 80% over 360 cycles at 1 C and 50 °C, compared to the standard LP30 liquid electrolyte (1 M $LiPF_6$ in ethylene carbonate : dimethyl carbonate (vol. 1:1)). [12, 17] More recently, a new family of pyrrolidinium-zwitterion OIPCs and their use in composite as solid electrolyte has been reported, which can increase target ion transport and support stable lithium metal cell cycling. [8, 26]

The OIPC/polymer composites have shown great promise as solid electrolytes. However, the OIPC/polymer composites made by pressing of the components (pellets) were brittle and needed to add liquid to support the contact between electrode and electrolyte. A facile preparation method that offers a flexible OIPC/polymer composite is required to achieve better electrode/electrolyte contact and thus enhanced electrochemical performance. Solution casting strategy is probably a good choice. There are only a few studies using solution casting method to prepare the OIPC/polymer composite reported. [27-29] Therefore, it is of importance to explore the OIPC/polymer composite prepared by solution casting method to advance the promise of the OIPC as solid electrolyte materials. Herein, the OIPC/polymer composites composed of the OIPC, 1-ethyl-1-methylpyrrolidinium bis(trifluoromethylsulfonyl)imide ($Pyr_{12}TFSI$), lithium bis(trifluoromethylsulfonyl)imide (LiTFSI) and PVDF were prepared by a straightforward solution casting method. Since using the solution casting method to prepare the OIPC/polymer composites is less studied, the impact of the composition on the properties of this composite electrolyte are ill-defined. Thus, the effect of the proportion of each component in the composites, including different molar proportions (10 mol% to 67 mol%) of LiTFSI in LiTFSI/$Pyr_{12}TFSI$ as well as different fractions (10 wt% - 50 wt%) of PVDF on the thermal property and ionic conductivity of the composites were initially determined. Free-standing and flexible OIPC/polymer composite films were obtained for the compositions with above 20 wt%

PVDF by the solution casting method. The advantage of this solution casting method is that it not only provides flexibility and better contact between electrode and electrolyte, but also is more compatible with current battery processing methods. Considering ionic mobility and mechanical strength, $Li_{0.33}Pyr_{0.67}TFSI$ and 30 wt% PVDF were chosen as the composition of the OIPC/polymer composite electrolyte for further investigations. The microscopic morphology, thermal stability and electrochemcial stability of the $Li_{0.33}Pyr_{0.67}TFSI$/30wt%PVDF composite film were characterized, and its application as solid electrolyte was evaluated in Li/Li symmetric cells as well as LFP/Li cells.

2. Experimental

2.1 Preparation of the OIPC/polymer composites

The OIPC/polymer composites were prepared by a solution casting method. LiTFSI (Solvionic, 99.9%, water content <20ppm) and $Pyr_{12}TFSI$ (Iolitec, 99%) in calculated mole ratios were mixed with corresponding amount of PVDF (Kynar 301F) in dimethoxyethane (DME) and sonicated for 10 min to form a homogeneous suspension. The suspension was stirred and heated at 100 °C for 90 s and then cast on a glass plate before drying under vacuum at 60 °C for 24 h. Self-standing and flexible composite films were obtained except for the composite with 10 wt% of PVDF, and the thickness of the resulting composite films measured by micrometer is about 150 μm.

2.2 Physicochemical characterization of the OIPC/polymer composites

The thermal behavior of the composites was characterized by differential scanning calorimetry (DSC) on a PerkinElmer DSC 6000 instrument. Samples of 3-4 mg were sealed in Al pan in an Ar-filled glovebox. The samples were cooled from room temperature to -50 °C and kept at

this temperature for 10 min. Then the samples were heated to 180 °C at a scan rate of 5 °C min^{-1}. The thermal stability of the composite was determined by thermogravimetric analysis (TGA) using a PerkinElmer TGA 8000 instrument equipped with an AccuPik sampler. The measurement was carried out on 5.5 mg sample sealed in Al pan in an Ar-filled glovebox, from 30 °C to 500 °C at a heating rate of 5 °C min^{-1} under argon atmosphere. X-Ray Diffraction (XRD) was performed on an Empyrean, Malvern Panalytical X-ray diffractometer to identify the crystallographic structure of the composite at room temperature and 50 °C. The data were collected using Mo Kα radiation source with 2θ from 1.5° to 20°. The morphology of the composite was examined by a JEOL JSM-7600F scanning electron microscope (SEM) coupled with an X-ray energy dispersive spectrometer (EDS) with a 5 kV accelerating voltage.

2.3 Electrochemical measurements of the OIPC/polymer composite electrolyte

A BioLogic VMP3 potentiostat was used for all electrochemical tests of the composite electrolytes. Those were done on CR2032 coin cells that were assembled in an Ar-filled glovebox. Lithium metal foil used here was purchased from Thermo Scientific Chemicals with a thickness of 0.75mm.

Ionic conductivity

The ionic conductivity of the composite electrolytes at different temperatures was measured by sandwiching the composite electrolyte between two stainless steel (SS) substrates in coin cells. The ionic conductivity plots were obtained by electrochemical impedance spectroscopy (EIS) with frequency range from 1 MHz to 0.5 Hz at temperatures from room temperature to 80 °C.

Linear sweep voltammetry (LSV)

The electrochemical stability of the composite electrolyte was tested with Li/SS cells through LSV from open circuit voltage (OCV) to 6.0 V at a scanning rate of 1.0 mV s^{-1} at room temperature.

Li/Li symmetric cell cycling

Li/Li symmetric cells were assembled to evaluate the compatibility and cycling stability of the composite electrolyte with lithium metal. The symmetric cells were cycled by galvanostatic charge-discharge technique at 50 °C. Meanwhile, EIS was also recorded at every 200 cycles to investigate the evolution of impedance.

LFP/Li cell assembly and cycling

The LFP electrode was prepared by a solution casting method. LFP, Carbon 65 and PVDF in a weight ratio of 8:1:1 were mixed in 1-methyl-2-pyrrolidone (NMP) and ball-milled for 4 h to form a homogeneous slurry. Then, the slurry was cast onto a carbon-coated aluminum current collector and dried at 110 °C under vacuum for 24h. Coin cells were assembled by stacking the LFP electrode as cathode, the OIPC/polymer composite film as electrolyte and Li metal as anode. The mass loading of LFP is around 1.5 mg cm^{-2} except that the amount for one test with higher loading of LFP was 3.1 mg cm^{-2}. The cycling performance of the LFP/Li cells with the composite electrolyte was evaluated by galvanostatic charge-discharge experiments at various C rates at 50 °C. All cells were kept at this temperature for 1 h before measurements to ensure homogeneous temperature of the cell. The cut-off voltage for the cycling of LFP/Li cells were from 2.5 V to 4.0 V.

3. Results and discussion

3.1 Thermal behavior

The thermal phase behavior of the OIPC/polymer composites with different compositions was investigated by DSC measurements. The influence of the concentration of LiTFSI on the thermal property of the composites was first studied. Figure 1a and b show the DSC traces of the composites containing different molar proportions (10 mol% to 67 mol%) of LiTFSI in LiTFSI/Pyr_{12}TFSI and 30 wt% PVDF, labeled Li_xPyr_yTFSI/30wt%PVDF (where x and y represent molar ratio between LiTFSI and Pyr_{12}TFSI). The traces for the pure components LiTFSI, Pyr_{12}TFSI and PVDF are also shown for comparison. The pure Pyr_{12}TFSI, as a representative OIPC, shows two solid-solid phase transitions at 15 °C and 45 °C before melting at 90 °C, which are consistent with the previous work. [9, 10] When the Pyr_{12}TFSI and LiTFSI are incorporated into the polymer PVDF to form composites, the thermal phase behavior of the composites is significantly changed. The endothermic peaks of the composites become broad and asymmetric in comparison with the neat components, especially for the peaks found in the temperature range between 10 °C and 50 °C, indicating that the introduction of LiTFSI and PVDF significantly enhances the disorder of OIPC. As the amount of LiTFSI is increased, the endothermic peaks are increasingly broadened, reflecting the effect of LiTFSI on the enhancement in the disorder of the OIPC. Meanwhile, the solid-solid phase transition peak at 45 °C is still clearly visible until high molar concentration (50 mol% and 67 mol%) of LiTFSI is reached. It is a well-known phenomenon that the melting point of OIPC might be lowered upon the addition of alkali metal salts such as Li salt. [11, 21, 30, 31] Here, when low molar concentration (10 mol%) of LiTFSI is used, the melting of the OIPC in the composite shifts to a lower temperature around 74 °C. The peak associated with melting of the composite disappears at higher LiTFSI concentrations (20 mol% and 33 mol%). There are two possibilities to explain this disappearance. The melting peak might further shift to a lower

temperature around 45 °C and become overlapped with the solid-solid phase transition peak. Alternatively, the melting peak may disappear as the OIPC in the composite does not melt but changes to an amorphous state. To better understand the phase transition around this temperature, the XRD measurement for the composite with 33 mol% LiTFSI ($Li_{0.33}Pyr_{0.67}TFSI$/30wt%PVDF) were conducted at room temperature and 50 °C, respectively. As shown in Figure S1, the XRD pattern of the composite at room temperature presents sharp diffraction peaks at 2θ = 4.6°, 5.0°, 7.8°, 11.8° and 15.8°, whereas these peaks disappear at 50 °C. This result confirmed the change from a crystalline phase at room temperature to an amorphous phase at 50 °C. It is worth noting that the diffraction peaks of the composite at room temperature do not match with either pure LiTFSI or pure $Pyr_{12}TFSI$, indicating a new crystalline phase formed by the solution casting method. Looking back at the DSC (Figure 1b), a new small peak appearing at 26 °C for the composite with 10 mol% LiTFSI and a new broad small peak at a similar temperature near 29 °C for the composite with 33 mol% LiTFSI are observed, which is probably attributed to the transition of an eutectic phase as reported for the LiTFSI-$Pyr_{12}TFSI$ systems. [9, 10] Thus, a slight amount of liquid phase is likely to coexist with the solid phase beyond this temperature, which may have a positive impact on the ionic mobility. When the LiTFSI molar concentration in the composite is very high (50 mol% and 67 mol%), the endothermic peaks are extremely broad and the melting transitions shift less to lower temperature compared with the composite with 33 mol% LiTFSI, i.e. ca. 68 °C for the composite with 50 mol% LiTFSI and ca. 83 °C for the composite with 67 mol% LiTFSI, respectively. In addition to the OIPC, the melting peak of PVDF and the solid-solid phase transition of LiTFSI in the composites that are broadened and superimposed with each other are also shifted to a lower temperature compared with that of pure PVDF and LiTFSI. This is indicative of the interactions between the PVDF and $Pyr_{12}TFSI$/LiTFSI, which may benefit the ion diffusion and electrochemical performance. [21, 24, 32, 33] Undeniably, since the solid-solid

phase transition peak, the eutectic transition peak, and the melting point of the composites are so broad and intensively overlapped, it is difficult to analyze each individual phase transition.

The effect of the weight fraction of PVDF on the thermal phase behavior of the composites was also studied. Figure 1c shows the DSC traces of the mixture of $Li_{0.33}Pyr_{0.67}TFSI$ (i.e. 0 wt% of PVDF) and the composites containing $Li_{0.33}Pyr_{0.67}TFSI$ and different fractions of PVDF (10 wt% - 50 wt%), labeled x wt%PVDF/$Li_{0.33}Pyr_{0.67}TFSI$ (where x represents the weight fraction of PVDF). The mixture of $Li_{0.33}Pyr_{0.67}TFSI$ presents a small solid-solid phase transition (phase III to phase II) peak at 15 °C and a sharp peak at 33 °C overlapped with a small broad peak centered at 43 °C. The sharp peak at 33 °C is likely assigned to the eutectic phase and the broad peak centered at 43 °C might be attributed to either the overlapped phase II to phase I transition peak and melting peak or only the phase II to phase I transition peak as discussed above. As the PVDF fraction is increased, the endothermic peaks of the composites in the temperature range between 10 °C and 50 °C are increasingly broadened and reduced in intensity. In particular, the eutectic peak (at 33 °C) is significantly suppressed for PVDF fraction of 30 wt% and above, and all endothermic peaks in the temperature range between 10 °C and 50 °C are no longer visible when 50 wt% of PVDF is added. Increasing the fraction of PVDF to higher values results in increased disorder of the OIPC and suppression of the phase transitions of the OIPC. In addition, the melting peak of PVDF and the solid-solid transition of LiTFSI in the composites that are broadened and superimposed with each other were also shifted to a lower temperature compared with that of pure PVDF and LiTFSI. Specifically, the overlapped peak shifts to lower temperature when less amount of PVDF is added, indicating the interactions between the PVDF and $Pyr_{12}TFSI$/LiTFSI are reduced with increasing addition of PVDF.

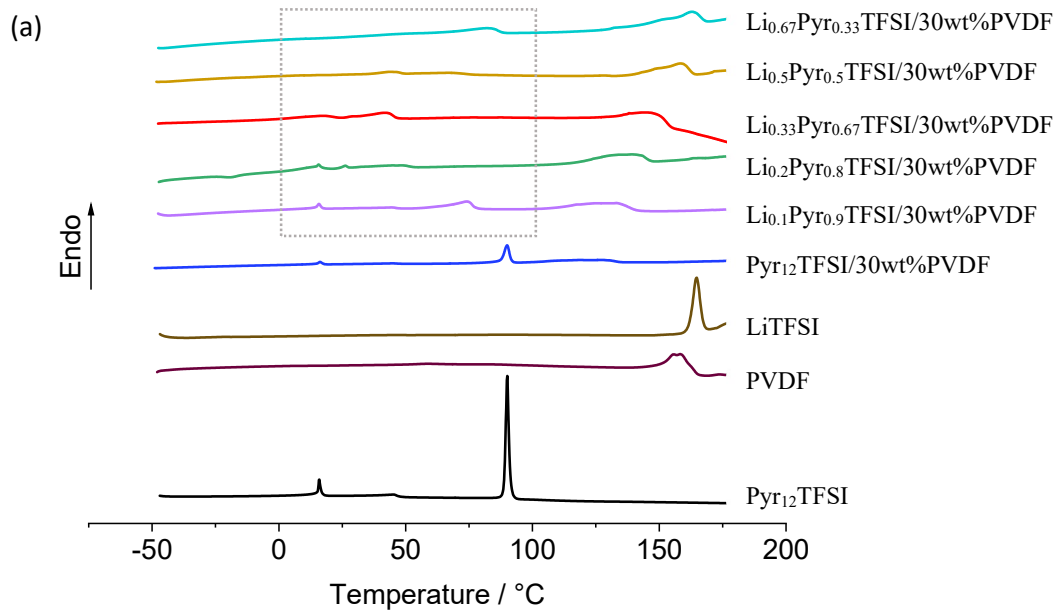

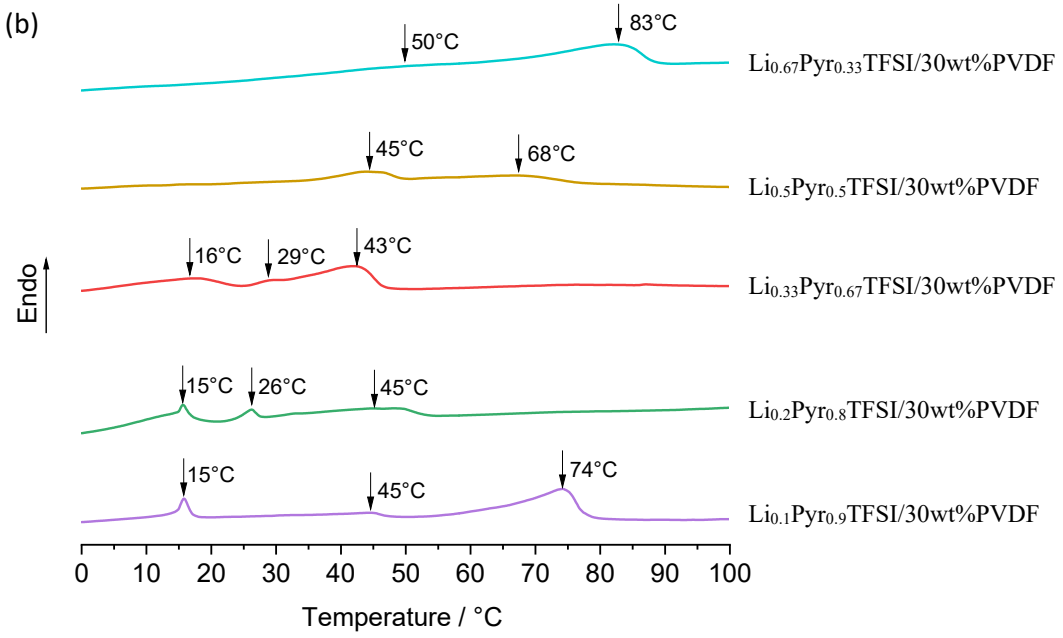

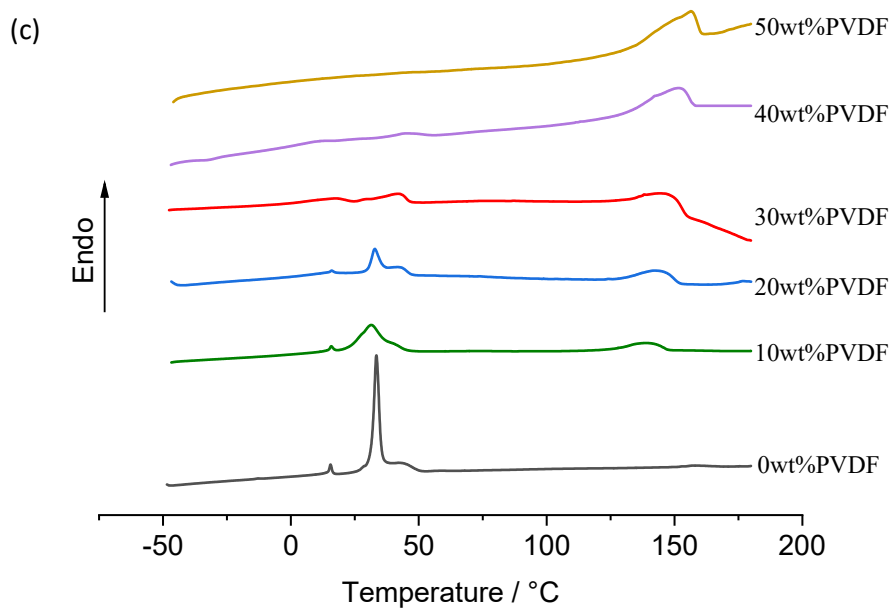

Figure 1. (a) DSC traces of pristine $Pyr_{12}TFSI$, LiTFSI, PVDF and the Li_xPyr_yTFSI/30wt%PVDF composites. (b) An enlargement of the curves in (a) in the temperature range between 0 °C and 100°C highlighting the temperature of the various transitions. (c) DSC traces of the mixture of the x wt%PVDF/$Li_{0.33}Pyr_{0.67}TFSI$ composites. The curves were scaled up by a magnification of 3 to better show the peaks. The samples were cooled from room temperature to -50 °C and kept at this temperature for 10 min. Then the samples were heated to 180 °C at a scan rate of 5 °C min^{-1}.

3.2 Ionic conductivity

The ionic conductivity of the OIPC/polymer composite electrolytes was calculated from the film resistance, which was measured by EIS experiments at varying temperatures from room temperature to 80 °C. The ionic conductivity of the composites containing different molar proportions (10 mol% to 67 mol%) of LiTFSI in LiTFSI/$Pyr_{12}TFSI$ and 30 wt% PVDF, i.e.

Li_xPyr_yTFSI/30wt%PVDF were studied at first. Figure 2a shows the Arrhenius plot for the ionic conductivity of the LiTFSI/30wt%PVDF composite, the $Pyr_{12}TFSI$/30wt%PVDF composite and the Li_xPyr_yTFSI/30wt%PVDF composites as a function of temperature. A linear relationship was obtained between the conductivity and temperature for the composites and could be fitted by the Arrhenius equation. The activation energy (E_a) values were calculated from the slope the curves in Figure 2a (shown in Table S1 of the Supporting Information). The composite with the lowest amount (10 mol%) of LiTFSI presents the highest activation energy of 0.51 eV. The ionic conduction activation energy of the other composites with high contents in Li salt (20 mol% and above) are very similar and the values are found between 0.21 and 0.32 eV. The $Pyr_{12}TFSI$/30wt%PVDF composite presents the lowest ionic conductivity in the measured temperature range, with a conductivity lower by up to two orders of magnitude than the other samples. This reflects that Li salt has a dominant effect on the ion transport of the composite electrolyte. This result is consistent with the poor dissociation of $Pyr_{12}TFSI$ by the polymer and the poor conductivity of the undoped OIPC. Adding LiTFSI into the composite highly enhanced the ionic conductivity, which is higher than the composites without either LiTFSI or $Pyr_{12}TFSI$ except the case of the composite with 10 mol% LiTFSI. The composite with 33 mol% LiTFSI shows the highest ionic conductivity values from room temperature to 50 °C among the studied composite compositions and the ionic conductivity value of this sample is promising in terms of solid electrolyte in Li battery applications. For example, the ionic conductivity of the sample is 1.2×10^{-4} S cm^{-1} at 30 °C and 4.2×10^{-4} S cm^{-1} at 50 °C, which is similar or higher compared to other OIPC-based electrolytes reported. [17, 21, 22] Therefore, the composition of $Li_{0.33}Pyr_{0.67}TFSI$ was chosen for the study of the effect of the PVDF fraction.

Figure 2b shows the Arrhenius plot for the ionic conductivity of the composites containing different weight fractions (20 wt% to 50 wt%) of PVDF and $Li_{0.33}Pyr_{0.67}TFSI$ as a function of temperature. The ionic conductivity of the composite with 20 wt% of PVDF presents a nonlinear dependency with temperature, which can be fitted by the Vogel–Fulcher–Tammann (VFT) equation. This nonlinear character is likely due to the obvious phase transitions occurring between room temperature to 50 °C. The conductivity of the composites with more than 30 wt% of PVDF increases nearly linearly with temperature as the phase transitions are hindered by the increasing fraction of PVDF, which is consistent with the above DSC results. The linear dependency can be fitted by the Arrhenius equation and the activation energy was calculated. The E_a values (0.21 to 0.27 eV) are close and similar to those obtained with 20 wt% LiTFSI and above with 30 wt% PVDF (Figure 2a). Increasing the fraction of PVDF leads to a decrease in ionic conductivity, suggesting that increasing loading of PVDF would impede the interconnected ion transport pathways.

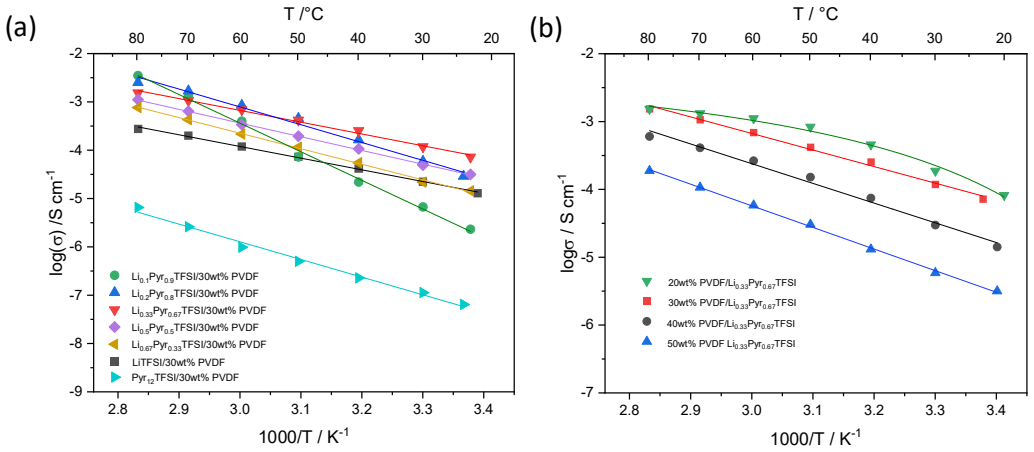

Figure 2. Ionic conductivity plot of (a) the LiTFSI/30wt%PVDF composite, the $Pyr_{12}TFSI$/30 wt%PVDF composite and the Li_xPyr_yTFSI/30wt%PVDF composites, and (b) the z wt%PVDF/$Li_{0.33}Pyr_{0.67}TFSI$ composites at varying temperatures from room temperature to 80 °C.

The utilization of adequate amounts of PVDF ensures strong mechanical integrity for composite electrolytes, a crucial factor for the long-term cycling of batteries. Figure S2 of the Supporting Information displays photographs of the $Li_{0.33}Pyr_{0.67}TFSI$ composites with different weight fractions of PVDF. The composites containing 10 wt% and 20 wt% of PVDF are transparent, while those containing 30 wt% and above form white films. The composite containing 10 wt% PVDF exhibits inadequate mechanical strength, making the formation of a free-standing film impossible. Similarly, the composite with 20 wt% PVDF is too brittle to serve as a solid electrolyte, despite being capable of forming a free-standing film. The $Li_{0.33}Pyr_{0.67}TFSI$/30wt%PVDF composite has the highest conductivity among the films that are strong enough to be incorporated in electrochemical cells. This composite was therefore selected for further physicochemical and electrochemical characterization.

3.3 Physicochemical characterization of the OIPC/polymer composite electrolyte

The $Li_{0.33}Pyr_{0.67}TFSI$/30wt%PVDF composite forms a self-standing and flexible white film as seen in Figure 1a and the microscopic morphology of the composite film is shown in Figure 1b-e. The flexibility and softness of the composite film provides good contact between the electrolyte and electrodes, which is beneficial for electrochemical performance. At the microscopic level, the pristine PVdF are discrete spherical nanoparticles with an average diameter of approx. 250 nm (Figure 1f). After the OIPC and lithium salt were added together with PVDF to prepare the composite film by solution-casting method, the OIPC and lithium salt are incorporated within the polymer matrix, forming a continuous porous network that is composed of spherical particles with diameter of about 2 micron, as illustrated in Figure 1b-d. The spherical particles are dispersed homogeneously and entangled with each other to form many pores (Figure 1c and d), which is also evenly distributed. The SEM observation

demonstrated that the solution-casting method can effectively result in a uniform dispersion of components. Chemical mapping was also performed by EDS, further supporting the homogeneity of elemental distribution of the composite electrolyte, as shown in Figure S4. The homogeneous distribution and porous network of the composite electrolyte are favorable for the Li-ion transport and further cycling performances. [34, 35]

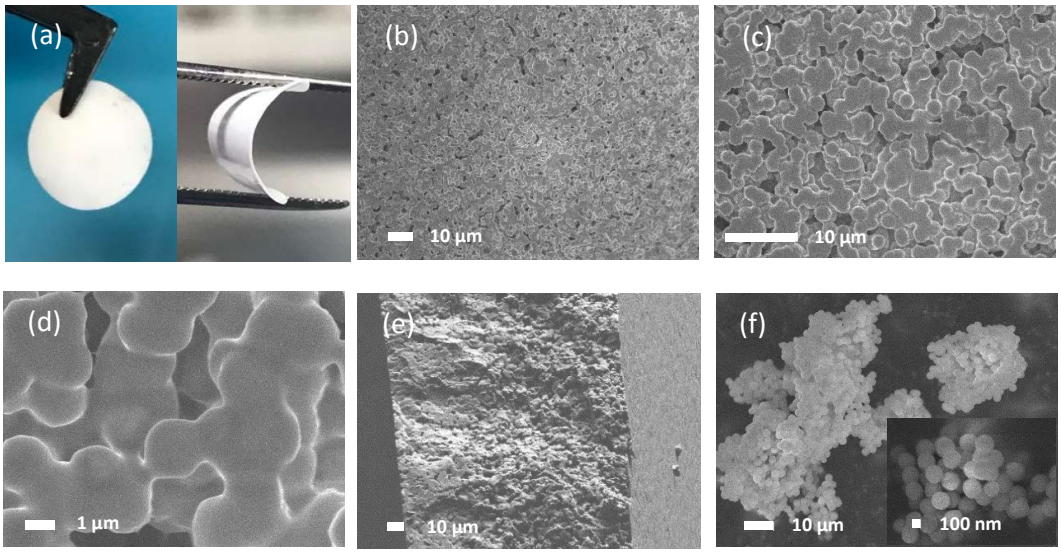

Figure 2. (a) Photographs of the flexible $Li_{0.33}Pyr_{0.67}TFSI$/30wt%PVDF composite film. SEM images of (b)-(d) the surface of the $Li_{0.33}Pyr_{0.67}TFSI$/30wt%PVDF composite film at different magnification, (e) the cross section of the composite film and (f) pristine PVDF.

TGA was used to study the thermal stability of the $Li_{0.33}Pyr_{0.67}TFSI$/30wt%PVDF composite film. The TGA profile in Figure S3 of the Supporting Information shows that no weight loss due to either decomposition or volatilization was observed until 280 °C, indicating a sufficient stability for battery applications. The TGA analysis also shows that DME solvent used during

the preparation process was successively removed by the vacuum treatment (see Experimental section). The high thermal stability of the composite electrolyte provides more safety for their applications in electrochemical devices.

3.4 Electrochemical stability against Li metal

To assess the applicability of the OIPC/polymer composite electrolyte for Li batteries, the electrochemical stability of the $Li_{0.33}Pyr_{0.67}TFSI$/30wt%PVDF composite electrolyte was firstly evaluated by LSV in a Li/SS cell. The linear sweep voltammogram (Figure S5) shows that the electrochemical stability of the composite electrolyte reaches 4.6 V, at which the current density increases above 2 μA cm^{-2}. The electrochemical stability of this composite electrolyte is close to the similar $Pyr_{12}FSI$/PVDF composite system prepared by powder pressing method [12, 17] and matches with the requirement of many high-voltage cathode materials.

Then, Li/Li symmetric cells were assembled to test the long-term cycling stability of lithium plating/stripping process with the $Li_{0.33}Pyr_{0.67}TFSI$/30wt%PVDF composite electrolyte. As seen in Figure 3a-c, the Li/Li symmetric cell cycled by galvanostatic charge-discharge experiment at a current density of 0.1 mA cm^{-2} at 50 °C exhibited stable voltage profiles for periods up to 900 h. The cell shows low overpotential, which was initially only 35 mV and remained as low as 62 mV after 900 h. There is no obvious voltage spike or sudden short circuit observed during cycling, demonstrating stable and uniform lithium plating/stripping process without short circuiting caused by severe Li dendrite growth. The Nyquist plot obtained during cycling in Figure 3d showed a slight increase in the intercept at the real impedance axis at high frequencies with the number of cycles. This increase in the cell resistance is probably due to the morphology evolution of electrolyte or the depletion of Li and electrolyte [36, 37]. A gradual

increase in the semi-circle radius associated with interfacial resistance is also noted, which is attributed to the formation of a stable solid electrolyte interphase (SEI) layer on the lithium anode [38, 39]. It has been demonstrated that a stable SEI layer can effectively mitigate against the loss and consumption of both active Li and electrolyte and suppress the growth of Li dendrite. [40, 41] Thus, these results not only reveal that the composite electrolyte can lead to homogeneous Li deposition/dissolution and effectively inhibit the Li dendrite growth-induced short circuiting, but also verify the applicability of the composite electrolyte with Li metal.

The rate capability of Li/Li symmetric cell with the composite electrolyte was also investigated, in which the cell was cycled with successive current densities from 0.05 to 0.35 mA cm^{-2} as seen in Figure 3e. The result indicates that the Li plating/stripping with the composite electrolyte can be stably operated at various current densities (0.05 to 0.3 mA cm^{-2}), while a higher current density of 0.35 mA cm^{-2} leads to cell failure.

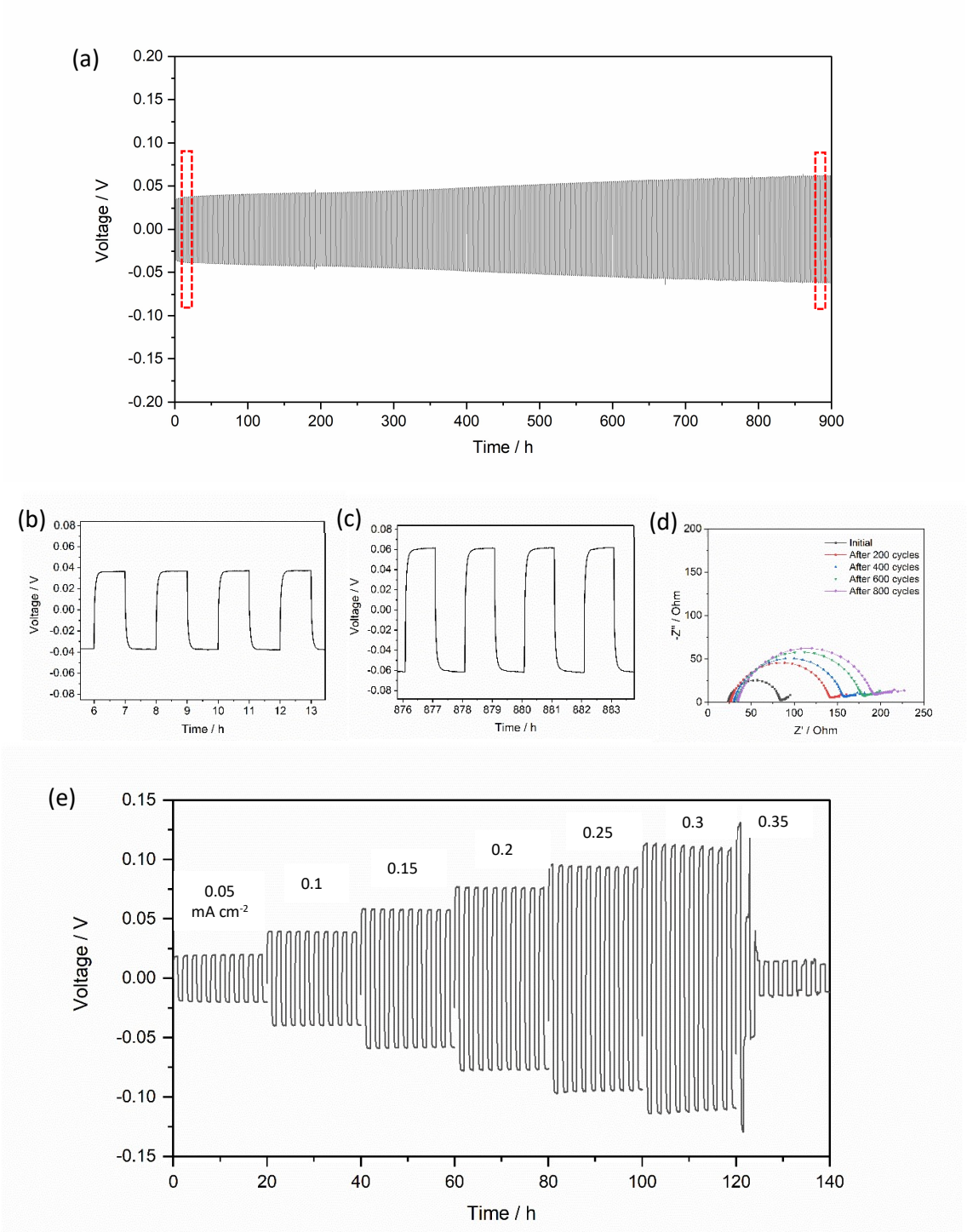

Figure 3. (a) Voltage profile of Li/Li symmetric cell cycling at 0.1 mA cm^{-2} at 50 °C with 1 h duration for each half cycle. (b, c) The detailed voltage profiles of Li/Li symmetric cell cycling at 0.1 mA cm^{-2} at 50 °C in different cycle stages highlighted by the red boxes in the full profile. (d) Nyquist plots of electrochemical impedance spectra during Li/Li symmetric cell cycling at

0.1 mA cm^{-2} at 50 °C. (e) Voltage profile of Li/Li symmetric cell cycling with increasing current density from 0.05 mA cm^{-2} to 0.35 mA cm^{-2} at 50 °C; 1 h duration for each half cycle and 10 cycles at each current density.

3.5 LFP/Li cell performance

Considering the good electrochemical stability of the composite electrolyte with Li metal, the $Li_{0.33}Pyr_{0.67}TFSI$/30wt%PVDF composite electrolyte was further tested in full cells with LFP as the cathode material and Li metal as the anode. The LFP/Li cell with the composite electrolyte was cycled at a range of C rates from 0.1 C to 2 C at 50 °C. As shown in Figure 4a and b, when the cell was cycled at 0.1 C and 0.2 C, it delivered high specific capacities of 149 mAh g^{-1} and 148 mAh g^{-1}, respectively. As 0.5 C, 1 C and 2 C were applied, the specific capacities were 142 mAh g^{-1}, 129 mAh g^{-1} and 56 mAh g^{-1}, respectively. When the charging rate was set back to 0.1 C afterwards, the discharge capacity recovered back to 151 mAh g^{-1}, a specific capacity value slightly higher than the initial capacity. A more stable capacity was noted after cycling at different rates, showing a stabilization period, although the resistance appeared to be higher as the profiles are less rectangular than that in the first 0.1 C cycles. The improvement of the capacity could come from more active material being accessible by the electrolyte and better contact between the membrane and the composite electrode. It is also worth noting that the cell with this composite electrolyte delivered higher capacities at 1 C and below in comparison with the $Pyr_{12}FSI$/PVDF composite electrolyte prepared by powder pressing method (maximum 128 mAh g^{-1}) [8-12], which is due to the higher flexibility of the film electrolyte allowing access to more material in the composite LFP cathode. Moreover, the LFP loading was doubled in the cathode (3.1 mg cm^{-2}), the cell can still maintain high capacities of 149 mAh g^{-1}, 145 mAh g^{-1} and 128 mAh g^{-1} at C rate ranging from 0.1 C to 0.5 C. The specific capacities were significantly lower (34 mAh g^{-1} and 21 mAh g^{-1}) at C rates of 1 C and 2 C, as

shown Figure S6a and b, due to the Li^+ transport limitation in the solid electrolyte. The cells with the composite electrolyte were also cycled at different C rates at ambient temperature (Figure S7a and b of the Supporting Information). In this case, the discharge capacities obtained were very low, (for example, 32 mAh g^{-1} at 0.1 C due to limited ionic conductivity and crystal phase of the composite electrolyte at ambient temperature. This is also supported by the high resistance observed on the charge-discharge profiles.

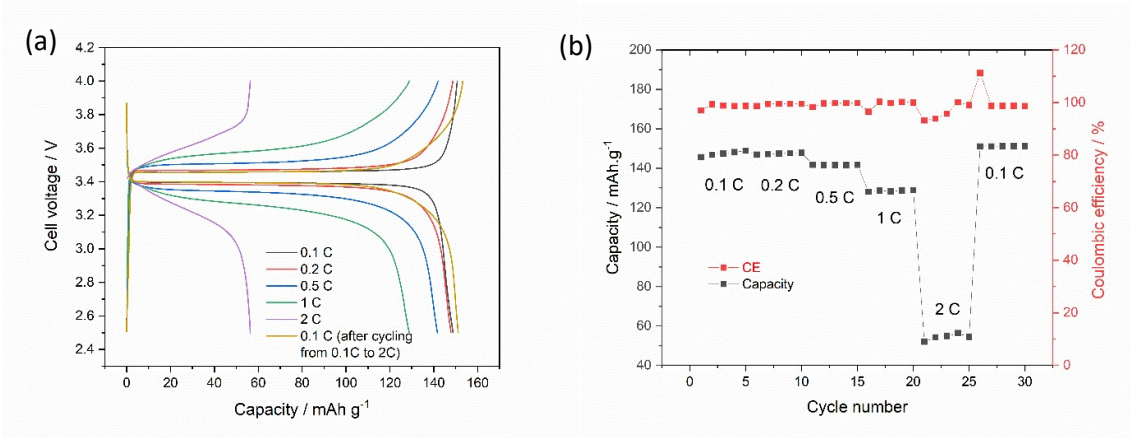

Figure 4. Electrochemical performances of the LFP/Li cells with the $Li_{0.33}Pyr_{0.67}TFSI$/30wt%PVDF composite electrolyte at 50 °C. The mass loading of LFP in the cathode is 1.5 mg cm^{-2}. (a) Voltage profile of the LFP/Li cell at different charging rates. (b) Rate performance of the LFP/Li cell at different charging rates.

The long-term cycling stability of the LFP/Li cell with the composite electrolyte at 0.5 C at 50 °C was further evaluated. The cell was cycled at low charging rate of 0.1 C for 5 cycles first for activation before being cycled at 0.5 C. As shown in Figure 5, the cell showed an initial discharge capacity of 136 mAh g^{-1} at 0.5 C, following a sharp drop in capacity to 133 mAh g^{-1} in the second cycle owing to the sudden change in charging rate. From the second cycle on, the cell was able to be cycled for 440 cycles with a capacity retention of 89 % and coulombic efficiency above 99.6%. The spike around 366 cycles is due to external factors (temperature

decrease caused by a power outage in the lab). It also noted that when the cell was cycled initially at 0.5 C without activation cycling at low C rate, the discharge capacity was low initially and gradually increased to 130 mAh g^{-1} over 30 cycles as shown in Figure S8. Despite the cycling performance of this cell not being as stable as the activated one, the capacity retention was superior (95 % retention over 430 cycles). The excellent rate performance and long-term cycling performance of the LFP/Li cell highlighted the great potential of this OIPC/polymer composite electrolyte in the application of Li batteries.

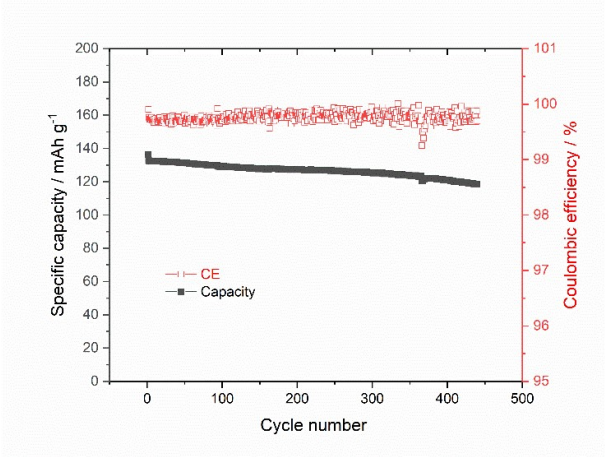

Figure 5. Long-term cycling performance of the LFP/Li cell with the $Li_{0.33}Pyr_{0.67}TFSI$/30wt%PVDF composite electrolyte at 0.5 C (initially at 0.1 C for 5 cycles) at 50 °C. The mass loading of LFP in the cathode is 1.5 mg cm^{-2}.

4. Conclusions

In summary, free-standing and flexible OIPC/polymer composite films were fabricated by a simple solution casting method. The thermal behavior and ionic conductivity of the composites with different proportions of components were investigated. Li salt concentration in the composites has distinct impacts on the thermal behavior and ionic conductivity of the

composites. Increasing loading of PVDF in the composites suppresses the phase transitions and reduces ionic conductivity of the composites. The OIPC/polymer composite electrolyte with a high Li salt concentration, i.e. $Li_{0.33}Pyr_{0.67}TFSI$/30wt%PVDF exhibited relatively high ionic conductivity (up to 10^{-4} S cm^{-1} at 30 °C) and was cycled stably in the Li/Li symmetric cell for more than 900 h at a current density of 0.1 mA cm^{-2} at 50 °C, showing a good compatibility with Li metal. The LFP/Li cell (1.5 mg cm^{-2} LFP in the cathode) with this OIPC/polymer composite electrolyte not only displayed excellent rate performance and particularly the discharge capacity of 149 mAh g^{-1} at 0.1 C at 50 °C, but also can sustain stable cycling for a long cycle life of over 440 cycles with capacity retention of 89% at 0.5 C at 50 °C. The $Li_{0.33}Pyr_{0.67}TFSI$/30wt%PVDF OIPC/polymer composite in this work shows great potential for their application as solid electrolyte in Li battery and the preparation strategy demonstrated here can be extended to other OIPC systems, opening an avenue to explore more high-performance OIPC-based composite electrolyte for Li battery and other battery devices.

Acknowledgements

The authors acknowledge the financial support of the Natural Sciences and Engineering Research Council of Canada (NSERC, Discovery grant program RGPIN-2019-05970) and the CQMF-QCAM (Quebec Center for Advanced Materials). YW acknowledges the Institut de l'Énergie Trottier for being awarded with a Graduate Scholarship.

References

(1) Tarascon, M. A. a. J.-M. Building Better Batteries. *Nature* **2008**, *451*, 652–657.

(2) Xia, S.; Wu, X.; Zhang, Z.; Cui, Y.; Liu, W. Practical Challenges and Future Perspectives of All-Solid-State Lithium-Metal Batteries. *Chem* **2019**, *5* (4), 753-785. DOI: 10.1016/j.chempr.2018.11.013.

(3) Wang, X.; Kerr, R.; Chen, F.; Goujon, N.; Pringle, J. M.; Mecerreyes, D.; Forsyth, M.; Howlett, P. C. Toward High-Energy-Density Lithium Metal Batteries: Opportunities and Challenges for Solid Organic Electrolytes. *Adv. Mater.* **2020**, *32* (18), e1905219. DOI: 10.1002/adma.201905219.

(4) Zhu, H.; MacFarlane, D. R.; Pringle, J. M.; Forsyth, M. Organic Ionic Plastic Crystals as Solid-State Electrolytes. *Trends Chem.* **2019**, *1* (1), 126-140. DOI: 10.1016/j.trechm.2019.01.002.

(5) Pringle, J. M.; Howlett, P. C.; MacFarlane, D. R.; Forsyth, M. Organic Ionic Plastic Crystals: Recent Advances. *J. Mater. Chem.* **2010**, *20* (11), 2056-2062. DOI: 10.1039/b920406g.

(6) Pringle, J. M. Recent Progress in the Development and Use of Organic Ionic Plastic Crystal Electrolytes. *Phys. Chem. Chem. Phys.* **2013**, *5* (15).

(7) Timmermans, J. Plastic Crystals: A Historical Review. *J. Phys. Chem. Solids* **1961**, *18*, 1-8.

(8) Makhlooghiazad, F.; O'Dell, L. A.; Porcarelli, L.; Forsyth, C.; Quazi, N.; Asadi, M.; Hutt, O.; Mecerreyes, D.; Forsyth, M.; Pringle, J. M. Zwitterionic Materials with Disorder and Plasticity and Their Application as Non-Volatile Solid or Liquid Electrolytes. *Nat. Mater.* **2022**, *21* (2), 228-236. DOI: 10.1038/s41563-021-01130-z.

(9) Forsyth, M.; Huang, J.; MacFarlane, D. R. Lithium Doped *N*-Methyl-*N*-Ethylpyrrolidinium Bis(Trifluoromethanesulfonyl)Amide Fast-Ion Conducting Plastic Crystals. *J. Mater. Chem.* **2000**, *10* (10), 2259-2265. DOI: 10.1039/b003168m.

(10) D.R. MacFarlane, J. H., M. Forsyth. Lithium-Doped Plastic Crystal Electrolytes Exhibiting Fast Ion Conduction for Secondary Batteries. *Nature* **1999**, *402*, 792–794.

(11) Zhou, Y.; Wang, X.; Zhu, H.; Yoshizawa-Fujita, M.; Miyachi, Y.; Armand, M.; Forsyth, M.; Greene, G. W.; Pringle, J. M.; Howlett, P. C. Solid-State Lithium Conductors for Lithium Metal Batteries Based on Electrospun Nanofiber/Plastic Crystal Composites. *Chemsuschem* **2017**, *10* (15), 3135-3145. DOI: 10.1002/cssc.201700691.

(12) Wang, X.; Zhu, H.; Greene, G. W.; Zhou, Y.; Yoshizawa-Fujita, M.; Miyachi, Y.; Armand, M.; Forsyth, M.; Pringle, J. M.; Howlett, P. C. Organic Ionic Plastic Crystal-Based Composite Electrolyte with Surface Enhanced Ion Transport and Its Use in All-Solid-State Lithium Batteries. *Adv. Mater. Technol.* **2017**, *2* (7). DOI: 10.1002/admt.201700046.

(13) Qian, J.; Henderson, W. A.; Xu, W.; Bhattacharya, P.; Engelhard, M.; Borodin, O.; Zhang, J. G. High Rate and Stable Cycling of Lithium Metal Anode. *Nat. Commun.* **2015**, *6*, 6362. DOI: 10.1038/ncomms7362.

(14) Suo, L.; Hu, Y. S.; Li, H.; Armand, M.; Chen, L. A New Class of Solvent-in-Salt Electrolyte for High-Energy Rechargeable Metallic Lithium Batteries. *Nat. Commun.* **2013**, *4*, 1481. DOI: 10.1038/ncomms2513.

(15) Wang, J.; Yamada, Y.; Sodeyama, K.; Chiang, C. H.; Tateyama, Y.; Yamada, A. Superconcentrated Electrolytes for a High-Voltage Lithium-Ion Battery. *Nat. Commun.* **2016**, *7*, 12032. DOI: 10.1038/ncomms12032.

(16) Matsumoto, K.; Inoue, K.; Nakahara, K.; Yuge, R.; Noguchi, T.; Utsugi, K. Suppression of Aluminum Corrosion by Using High Concentration LiTFSI Electrolyte. *J. Power Sources* **2013**, *231*, 234-238. DOI: 10.1016/j.jpowsour.2012.12.028.

(17) Zhou, Y.; Wang, X.; Zhu, H.; Armand, M.; Forsyth, M.; Greene, G. W.; Pringle, J. M.; Howlett, P. C. Ternary Lithium-Salt Organic Ionic Plastic Crystal Polymer Composite Electrolytes for High Voltage, All-Solid-State Batteries. *Energy Storage Mater.* **2018**, *15*, 407-414. DOI: 10.1016/j.ensm.2018.07.017.

(18) Zhou, D.; Shanmukaraj, D.; Tkacheva, A.; Armand, M.; Wang, G. Polymer Electrolytes for Lithium-Based Batteries: Advances and Prospects. *Chem* **2019**, *5* (9), 2326-2352. DOI: 10.1016/j.chempr.2019.05.009.

(19) Yang, Q.; Zhang, Z.; Sun, X. G.; Hu, Y. S.; Xing, H.; Dai, S. Ionic Liquids and Derived Materials for Lithium and Sodium Batteries. *Chem. Soc. Rev.* **2018**, *47* (6), 2020-2064. DOI: 10.1039/c7cs00464h.

(20) Fang, Z.; Zhao, M.; Peng, Y.; Guan, S. Organic Ionic Plastic Crystal Enhanced Interface Compatibility of PEO-Based Solid Polymer Electrolytes for Lithium-Metal Batteries. *Solid State Ion.* **2021**, *373*. DOI: 10.1016/j.ssi.2021.115806.

(21) Zhou, Y.; Wang, X.; Zhu, H.; Armand, M.; Forsyth, M.; Greene, G. W.; Pringle, J. M.; Howlett, P. C. *N*-Ethyl-*N*-Methylpyrrolidinium Bis(Fluorosulfonyl)Imide-Electrospun Polyvinylidene Fluoride Composite Electrolytes: Characterization and Lithium Cell Studies. *Phys. Chem. Chem. Phys.* **2017**, *19* (3), 2225-2234. DOI: 10.1039/c6cp07415d.

(22) Howlett, P. C.; Ponzio, F.; Fang, J.; Lin, T.; Jin, L.; Iranipour, N.; Efthimiadis, J. Thin and Flexible Solid-State Organic Ionic Plastic Crystal-Polymer Nanofibre Composite Electrolytes for Device Applications. *Phys. Chem. Chem. Phys.* **2013**, *15* (33), 13784-13789. DOI: 10.1039/c3cp51986d.

(23) Wang, X.; Zhu, H.; Greene, G. W.; Li, J.; Iranipour, N.; Garnier, C.; Fang, J.; Armand, M.; Forsyth, M.; Pringle, J. M.; et al. Enhancement of Ion Dynamics in Organic Ionic Plastic Crystal/PVDF Composite Electrolytes Prepared by Co-Electrospinning. *J. Mater. Chem. A* **2016**, *4* (25), 9873-9880. DOI: 10.1039/c6ta02817a.

(24) Iranipour, N.; Gunzelmann, D. J.; Seeber, A.; Vongsvivut, J.; Doherty, C.; Ponzio, F.; O'Dell, L. A.; Hollenkamp, A. F.; Forsyth, M.; Howlett, P. C. Ionic Transport through a Composite Structure of *N*-Ethyl-*N*-Methylpyrrolidinium Tetrafluoroborate Organic Ionic Plastic Crystals Reinforced with Polymer Nanofibres. *J. Mater. Chem. A* **2015**, *3* (11), 6038-6052. DOI: 10.1039/c4ta07155g.

(25) García, Y.; Porcarelli, L.; Zhu, H.; Mecerreyes, D.; Forsyth, M.; O'Dell, L. A. Physical Properties and Ion Dynamics in Composites of the Organic Ionic Plastic Crystal *N*-Ethyl-*N*-Methylpyrrolidinium Bis(Fluorosulfonyl)Amide with Lithium Sulphonamide Functional Acrylate Polymer Nanoparticles. *J. Mater. Chem. A* **2024**, *12* (7), 4146-4158. DOI: 10.1039/d3ta05698h.

(26) Makhlooghiazad, F.; Porcarelli, L.; Mecerreyes, D.; Forsyth, M.; O'Dell, L. A.; Pringle, J. M. Composite Lithium Conducting Solid Electrolytes Based on Zwitterionic Plastic Crystals and Polymer Nanoparticles. *Mater. Adv.* **2024**, *5* (7), 2841-2850. DOI: 10.1039/d3ma01156a.

(27) Liao, Z.; Huang, J.; Chen, W.; Saito, N.; Zhang, Z.; Yang, L.; Hirano, S.I. Safe, Superionic Conductive and Flexible "Polymer-in-Plastic Salts" Electrolytes for Dendrite-Free Lithium Metal Batteries. *Energy Storage Mater.* **2020**, *33*, 442-451. DOI: 10.1016/j.ensm.2020.09.003.

(28) Yang, K.; Zhang, Z.; Liao, Z.; Yang, L.; Hirano, S. I. Organic Ionic Plastic Crystal-Polymer Solid Electrolytes with High Ionic Conductivity and Mechanical Ability for Solid-State Lithium Ion Batteries. *ChemistrySelect* **2018**, *3* (44), 12595-12599. DOI: 10.1002/slct.201803094.

(29) Kim, E.; Jamal, H.; Jeon, I.; Khan, F.; Chun, S. E.; Kim, J. H. Functionality of 1-Butyl-2,3-Dimethylimidazolium Bromide (BMI-Br) as a Solid Plasticizer in PEO-Based Polymer

Electrolyte for Highly Reliable Lithium Metal Batteries. *Adv. Energy Mater.* **2023**, *13* (47). DOI: 10.1002/aenm.202301674.

(30) Makhlooghiazad, F.; Howlett, P. C.; Wang, X.; Hilder, M.; MacFarlane, D. R.; Armand, M.; Forsyth, M. Phosphonium Plastic Crystal Salt Alloyed with a Sodium Salt as a Solid-State Electrolyte for Sodium Devices: Phase Behaviour and Electrochemical Performance. *J. Mater. Chem. A* **2017**, *5* (12), 5770-5780. DOI: 10.1039/c6ta10340e.

(31) Al-Masri, D.; Yunis, R.; Hollenkamp, A. F.; Pringle, J. M. A Symmetrical Ionic Liquid/Li Salt System for Rapid Ion Transport and Stable Lithium Electrochemistry. *Chem. Comm.* **2018**, *54* (29), 3660-3663. DOI: 10.1039/c8cc00531a.

(32) Nti, F.; Greene, G. W.; Zhu, H.; Howlett, P. C.; Forsyth, M.; Wang, X. Anion Effects on the Properties of OIPC/PVDF Composites. *Mater. Adv.* **2021**, *2* (5), 1683-1694. DOI: 10.1039/d0ma00992j.

(33) Nti, F.; Porcarelli, L.; Greene, G. W.; Zhu, H.; Makhlooghiazad, F.; Mecerreyes, D.; Howlett, P. C.; Forsyth, M.; Wang, X. The Influence of Interfacial Interactions on the Conductivity and Phase Behaviour of Organic Ionic Plastic Crystal/Polymer Nanoparticle Composite Electrolytes. *J. Mater. Chem. A* **2020**, *8* (10), 5350-5362. DOI: 10.1039/c9ta12827a.

(34) Tang, S.; Guo, W.; Fu, Y. Advances in Composite Polymer Electrolytes for Lithium Batteries and Beyond. *Adv. Energy Mater.* **2020**, *11* (2). DOI: 10.1002/aenm.202000802.

(35) Costa, C. M.; Lee, Y.-H.; Kim, J.-H.; Lee, S.-Y.; Lanceros-Méndez, S. Recent Advances on Separator Membranes for Lithium-Ion Battery Applications: From Porous Membranes to Solid Electrolytes. *Energy Storage Mater.* **2019**, *22*, 346-375. DOI: 10.1016/j.ensm.2019.07.024.

(36) Zheng, J.; Engelhard, M. H.; Mei, D.; Jiao, S.; Polzin, B. J.; Zhang, J.-G.; Xu, W. Electrolyte Additive Enabled Fast Charging and Stable Cycling Lithium Metal Batteries. *Nat. Ener.* **2017**, *2* (3). DOI: 10.1038/nenergy.2017.12.

(37) Hongahally Basappa, R.; Ito, T.; Morimura, T.; Bekarevich, R.; Mitsuishi, K.; Yamada, H. Grain Boundary Modification to Suppress Lithium Penetration through Garnet-Type Solid Electrolyte. *J. Power Sources* **2017**, *363*, 145-152. DOI: 10.1016/j.jpowsour.2017.07.088.

(38) A. S. Best, A. I. B., and A. F. Hollenkamp. Ionic Liquids with the Bis(Fluorosulfonyl)Imide Anion: Electrochemical Properties and Applications in Battery Technology. *J. Electrochem. Soc.* **2010**, *27*, A903-A911. DOI: 10.1149/1.3429886.

(39) Bieker, G.; Winter, M.; Bieker, P. Electrochemical in Situ Investigations of SEI and Dendrite Formation on the Lithium Metal Anode. *Phys. Chem. Chem. Phys.* **2015**, *17* (14), 8670-8679. DOI: 10.1039/c4cp05865h.

(40) Li, S.; Zhang, S. Q.; Shen, L.; Liu, Q.; Ma, J. B.; Lv, W.; He, Y. B.; Yang, Q. H. Progress and Perspective of Ceramic/Polymer Composite Solid Electrolytes for Lithium Batteries. *Adv. Sci.* **2020**, *7* (5), 1903088. DOI: 10.1002/advs.201903088.

(41) Lin, R.; He, Y.; Wang, C.; Zou, P.; Hu, E.; Yang, X. Q.; Xu, K.; Xin, H. L. Characterization of the Structure and Chemistry of the Solid-Electrolyte Interface by Cryo-Em Leads to High-Performance Solid-State Li-Metal Batteries. *Nat. Nanotechnol.* **2022**, *17* (7), 768-776. DOI: 10.1038/s41565-022-01148-7.